A Monte Carlo uncertainty analysis of ozone trend predictions in a two-dimensional model

D. B. Considine,[1,2] R. S. Stolarski,[2] S. M. Hollandsworth,[2,3] C. H. Jackman,[2] and E. L. Fleming,[2,3]

Abstract. We use Monte Carlo analysis to estimate the uncertainty in predictions of total O_3 trends between 1979 and 1995 made by the Goddard Space Flight Center (GSFC) two-dimensional (2-D) model of stratospheric photochemistry and dynamics. The uncertainty is caused by gas phase chemical reaction rates, photolysis coefficients, and heterogeneous reaction parameters which are model inputs. The uncertainty represents a lower bound to the total model uncertainty assuming the input parameter uncertainties are characterized correctly. Each of the Monte Carlo runs was initialized in 1970 and integrated for 26 model years through the end of 1995. This was repeated 419 times using input parameter sets generated by Latin hypercube sampling. The standard deviation (σ) of the Monte Carlo ensemble of total O_3 trend predictions is used to quantify the model uncertainty. The 34% difference between the model trend in globally and annually averaged total O_3 using nominal inputs and atmospheric trends calculated from Nimbus 7 and Meteor 3 total ozone mapping spectrometer (TOMS) version 7 data is less than the 46% calculated 1σ model uncertainty, so there is no significant difference between the modeled and observed trends. In the northern hemisphere midlatitude spring the modeled and observed total O_3 trends differ by more than 1σ but less than 2σ, which we refer to as marginal significance. We perform a multiple linear regression analysis of the runs which suggests that only a few of the model reactions contribute significantly to the variance in the model predictions. The lack of significance in these comparisons suggests that they are of questionable use as guides for continuing model development. Large model/measurement differences which are many multiples of the input parameter uncertainty are seen in the meridional gradients of the trend and the peak-to-peak variations in the trends over an annual cycle. These discrepancies unambiguously indicate model formulation problems and provide a measure of model performance which can be used in attempts to improve such models.

1. Introduction

Two dimensional (2-D) models of stratospheric photochemistry and dynamics are used to study the changes that have occurred in column O_3 levels over the past 2 decades and the factors responsible for those changes. The models are valuable for these studies because they are simple enough to be run for many years, but still

[1]Department of Meteorology, University of Maryland, College Park.

[2]NASA Goddard Space Flight Center, Greenbelt, Maryland.

[3]Steven Myers and Associates Corporation, Vienna, Virginia.

describe the seasonal, meridional, and vertical structure of the atmosphere.

Comparison of 2-D model predicted total O_3 changes with observations tests the adequacy of our understanding of the processes that have modified atmospheric O_3 concentrations recently. Model/observation discrepancies are often taken as an indication that the model is incorrect and some important process is missing from the model formulation and our understanding. For instance, *Solomon et al.* [1996] noted that the agreement between the total O_3 time series calculated from total ozone mapping spectrometer (TOMS) data and a 2-D model was significantly improved by adding to the model a background sulfate aerosol layer which reproduced observed variations of the aerosol layer over the TOMS observing period. *Jackman et al.* [1996] included a parameterization of solar ultraviolet flux variations in addition to a realistically varying background sulfate aerosol and also found better agreement between

the model and observations. And recently, *Solomon et al.* [1998] found that including temperature fluctuations about the zonal mean made the modeled and observed total O_3 time series agree better in the northern hemisphere midlatitudes during springtime.

This "standard" method of utilizing 2-D models to interpret observations has proved fruitful but is limited because uncertainties in the values of model input parameters such as chemical reaction rates result in uncertain model output. If this uncertainty is large compared to a model/measurement discrepancy, then no significance can be attributed to the difference, as it might easily be due to an input parameter error rather than a problem with the model formulation.

The propagation of input parameter uncertainties through atmospheric photochemistry and dynamics models is time-consuming but straightforward. The most common method to date is the Monte Carlo technique [*Stolarski et al.*, 1978; *Stolarski and Douglass*, 1986; *Douglass and Stolarski*, 1987; *Thompson and Stewart*, 1991; *Gao et al.*, 1996; *Stewart and Thompson*, 1996; *Chen et al.*, 1997; *Fish and Burton*, 1997]. There has not been a great deal of work in this area, perhaps because it is generally felt that many important processes such as those controlling atmospheric transport are so crudely parameterized that input parameter uncertainties are likely to be small in comparison. Although this may be true, the goal of this paper is to quantitatively assess the uncertainty in 2-D model predictions of O_3 trends and to use this information to interpret comparisons between the model predictions and TOMS observations of trends in total O_3. If a model/measurement discrepancy is rendered insignificant by known uncertainties in the input parameters, additional unquantified sources of uncertainty will not affect this result.

In this paper we use a Monte Carlo technique to evaluate the uncertainty in the O_3 trend predictions of the NASA Goddard Space Flight Center (GSFC) 2-D model. We consider the effects of uncertainties in chemical reaction rates, photolysis coefficients, and heterogeneous reaction rates. The model includes a parameterization of the solar cycle variation and a realistic variation of the sulfate aerosol surface area density between 1979 and 1995. In section 2 we briefly describe the version of the GSFC 2-D model used in these studies. In section 3 we discuss the Monte Carlo method and details of the runs analyzed in this paper. In section 4 we present the results of the Monte Carlo uncertainty analysis. We summarize our results and draw some conclusions in section 5.

2. Model Description

The Goddard Space Flight Center 2-D model has been described fairly completely in numerous previous publications [e.g., Jackman *et al.*, 1996, and references therein]. We briefly summarize its features here.

The model has a $10°$ latitudinal resolution, with the midpoints of the 18 latitude bands located at $-85°, \ldots, +85°$. The vertical coordinate is log-pressure with a resolution of about 2 km. The model uses the residual circulation formulation described by *Fleming et al.* [1995]. Constituents are advected using the second-order moment scheme of *Prather* [1986]. Note that the *Jackman et al.* [1996] study uses a somewhat different residual circulation formulation and a piecewise-parabolic advection scheme instead of second-order moments. These differences do not affect the conclusions of this study.

The model contains a fairly complete description of stratospheric chemical processes. It calculates the concentrations of 62 species. Of these, 28 are transported, and the remainder are calculated using photochemical equilibrium assumptions. Family approximations are used for O_x, NO_x, ClO_x, and Br_x species. There are 106 gas phase chemical reactions in the model chemical scheme. The reaction rates are calculated from values specified by *DeMore et al.* [1994].

Heterogeneous reactions occur on a background sulfate aerosol layer. The sulfate aerosol surface area density distribution used to calculate the reaction rates is based on satellite extinction measurements made between 1979 and 1995 as described by *Jackman et al.* [1996]. The distribution represents the temporal variation of the zonal mean atmospheric sulfate aerosol layer in response to the various volcanic eruptions which have occurred since 1979. Heterogeneous reactions on Type 1 (nitric acid trihydrate) and Type 2 (water ice) polar stratospheric clouds (PSCs) are also included. The PSC surface area densities are calculated following *Considine et al.* [1994]. All of the heterogeneous reactions included in the model are included in the Monte Carlo input parameter set described in section 3.

There are 45 photolytic decomposition reactions included in the model. The photolysis coefficients are specified from a photolytic source term look-up table generated with the Anderson radiation code described by *Anderson and Lloyd* [1990]. Cross sections are taken from *DeMore et al.* [1994]. The model also includes a parameterization of solar cycle variations in the solar UV flux, again as described by *Jackman et al.* [1996].

3. Monte Carlo Methodology

In a Monte Carlo analysis of the uncertainty in a particular model output, the model is run many times using a different set of input parameter values in each run. Each set is a combination of possibly correct input parameter values which are chosen on the basis of the specified uncertainty in each of the input parameters. Each input parameter value set results in different model output. The ensemble of model output values produced by the Monte Carlo runs is then used to characterize the output uncertainty resulting from uncertainties in the input parameters.

3.1. Parameters

Table 1 lists the 93 chemical reactions whose uncertainties are propagated through the model in this study. Since the model includes 106 gas phase reactions in all, 13 reactions are not included as Monte Carlo parameters. These reactions are only important in the mesosphere, so their neglect has no bearing on the study of uncertainty in total O_3 predictions.

To understand how values used in the Monte Carlo runs are chosen for a particular reaction, consider a bimolecular reaction with the Arrhenius form,

$$k(T) = A \exp \left(\frac{-E}{R} \left(\frac{1}{T} \right) \right), \qquad (1)$$

where $k(T)$ is the reaction rate at temperature T, A is a constant, and E/R is the activation energy in kelvins. To make the discussion below easier to follow, note that this can be rewritten in terms of the reaction rate at 298 K, k_{298}:

$$k(T) = k_{298} \exp \left(\frac{E}{R} \left(\frac{1}{298} - \frac{1}{T} \right) \right). \qquad (2)$$

Both k_{298} and E/R are measured quantities and therefore are uncertain. In a Monte Carlo study, these uncertainties are represented with probability distributions which are then sampled in some way to obtain the set of values used in the Monte Carlo runs.

DeMore et al. [1994] provides an estimate of the uncertainty of k_{298} and E/R, denoted f_{298}, and $\Delta E/R$, respectively. The publication also provides an equation for determining the uncertainty in the reaction at any temperature T,

$$f(T) = f_{298} \exp \left| \frac{\Delta E}{R} \left(\frac{1}{T} - \frac{1}{298} \right) \right|. \qquad (3)$$

This expression cannot be used directly in a Monte Carlo study because it implies a different probability distribution characterizing the reaction uncertainty at each temperature. Sampling multiple probability distributions to obtain rates for a single reaction would destroy the Arrhenius form of the reaction rate.

In this paper we assume that the uncertainty in k_{298} is described by a lognormal probability distribution and the uncertainty in E/R is described by a normal distribution. A lognormal distribution is chosen for k_{298} to exclude choosing negative values for this quantity, which would be physically unrealistic. No such constraint exists for E/R, so we characterize its uncertainty using a normal distribution with mean E^0/R and standard deviation $\Delta E/R$ taken from DeMore et al. [1994].

The upper uncertainty bound for k_{298} is specified in DeMore et al. [1994] by $k_{298}^+ = k_{298}^0 f_{298}$, where k_{298}^0 is the nominal value of the rate. Taking the logarithm of this relationship results in,

$$\ln(k_{298}^+) = \ln(k_{298}^0) + \ln(f_{298}). \qquad (4)$$

Since the upper uncertainty bound of a quantity is

typically specified as one standard deviation above its mean value, this form suggests that we can describe the uncertainty in the logarithm of k_{298} by a normal distribution with a mean of $\ln(k_{298}^0)$ and standard deviation $\ln(f_{298})$. With this choice the uncertainty in k_{298} is described by the lognormal distribution:

$$P(k_{298}) = C \exp \left(\frac{-\ln^2 \left(k_{298}/k_{298}^0 \right)}{2 \ln^2 (f_{298})} \right), \qquad (5)$$

where

$$C = \frac{1}{(2\pi)^{1/2} (k_{298} \ln(f_{298}))}. \qquad (6)$$

To choose a rate for a bimolecular reaction in a Monte Carlo run, a value for k_{298} is chosen by sampling equation (5) and a value for E/R is chosen by sampling the normal distribution describing its uncertainty. The rate of the reaction for that Monte Carlo run is then constructed from equation (2). This method preserves the Arrhenius form of the bimolecular reaction rates, as desired.

It should be noted that DeMore et al. [1994] do not provide a specific definition of the uncertainty bounds listed in the document. The publication instead states that the uncertainties are subjective and are not based on a rigorous statistical analysis of the available measurements for each rate. The interpretation of these limits we have adopted in this paper is therefore our own. While reasonable, it is not unique. For instance, Stewart and Thomson [1996] made the identification $f_{298} = 1 + s/m$, where s and m are the mean and standard deviation of the lognormal distribution characterizing the uncertainty in k_{298}. With this reasonable assumption, the standard deviation of $\ln(k_{298})$ is not $\ln(f_{298})$ as we assume but $\{\ln[1 + (f_{298} - 1)^2]\}^{(1/2)}$. This function increases slightly faster than $\ln(f_{298})$ as f_{298} increases, but not significantly so.

Termolecular reactions are treated similarly to the bimolecular case. DeMore et al. [1994] provide the functional form for a termolecular reaction in the low-pressure limit,

$$k_0(T) = k_0^{300}[M] \left(\frac{T}{300} \right)^{-n}, \qquad (7)$$

where $[M]$ is the number density of air, and $k_0^{300}[M]$ is the effective bimolecular rate of the reaction at 300 K in the low-pressure limit. DeMore et al. [1994] also provide uncertainty estimates Δk_0^{300} and Δn for k_0^{300} and n, respectively. We generate a lognormal distribution from k_0^{300} and Δk_0^{300} from which to pick values for the Monte Carlo runs and a normal distribution from n and Δn. For simplicity, we have ignored the uncertainty of the termolecular reactions in the high pressure limit. Thus, the uncertainty distributions generated for the termolecular reactions underestimate the uncertainty in these reactions implied by the DeMore et al. [1994] values.

Table 1. Gas Phase Reactions Varied in Monte Carlo Runs

Parameter	Description	f_{298} or Δk_0^{300}	$\Delta E/R$ or Δn
R1	$O + O_2 + M \to O_3 + M$	5E-35	0.5
R2	$O + O_3 \to 2O_2$	1.15	250
R3	$H + O_2 + M \to HO_2 + M$	5E-33	0.5
R4	$OH + O_3 \to HO_2 + O_2$	1.3	300
R5	$HO_2 + O_3 \to OH + 2O_2$	1.3	500
R6	$ClO + HO_2 \to HOCl + O_2$	1.4	250
R7	$Cl + H_2O_2 \to HCl + HO_2$	1.5	500
R8	$O(^1D) + M \to O(^3P) + M$	1.2	100
R9	$NO + O_3 \to NO_2 + O_2$	1.2	200
R10	$NO_2 + O_3 \to NO_3 + O_2$	1.15	150
R11	$H + O_3 \to OH + O_2$	1.25	200
R12	$OH + OH + M \to H_2O_2 + M$	3.0E-31	2.0
R13	$OH + ClONO_2 \to HOCl + NO_3$	1.5	200
R14	$CH_4 + OH \to CH_3 + H_2O$	1.1	150
R15	$CH_3O_2 + NO \to CH_3O + NO_2$	1.5	180
R16	$OH + CH_3Cl \to H_2O + CH_2Cl$	1.2	250
R17	$CH_3O + O_2 \to CH_2O + HO_2$	1.5	300
R18	$OH + NO_2 + M \to HNO_3 + M$	3E-31	0.7
R19	$HO_2 + HO_2 \to H_2O_2 + O_2$	1.3	200
R20	$N + O_2 \to NO + O$	1.25	400
R21	$CH_2O + O \to HCO + OH$	1.25	250
R22	$CH_3O_2 + HO_2 \to CH_3OOH + O_2$	2.0	400
R23	$Cl + H_2 \to HCl + H$	1.25	200
R24	$Cl + O_3 \to ClO + O_2$	1.15	100
R25	$ClO + O \to Cl + O_2$	1.3	70
R26	$Cl + CH_4 \to HCl + CH_3$	1.1	150
R27	$HCl + OH \to Cl + H_2O$	1.3	100
R28	$ClO + NO \to Cl + NO_2$	1.15	100
R29	$H_2O_2 + OH \to H_2O + HO_2$	1.2	100
R30	$H_2 + OH \to H_2O + H$	1.2	400
R31	$N_2O_5 + M \to NO_2 + NO_3 + M$	1.3	500
R32	$ClO + NO_2 + M \to ClONO_2 + M$	3E-32	1.0
R33	$H_2O_2 + O \to HO_2 + OH$	2.0	1000
R34	$HO_2 + NO_2 + M \to HO_2NO_2 + M$	3E-32	0.4
R35	$ClONO_2 + O \to ClO + NO_3$	1.5	200
R36	$HNO_3 + OH \to NO_3 + H_2O$	1.3	100
R37	$NO + HO_2 \to OH + NO_2$	1.2	80
R38	$H_2O + O(^1D) \to 2OH$	1.2	100
R39	$OH + HO_2 \to H_2O + O_2$	1.3	200
R40	$OH + O \to H + O_2$	1.2	100
R41	$HO_2 + O \to OH + O_2$	1.2	100
R42	$NO_2 + O \to NO + O_2$	1.1	120
R43	$NO_2 + O + M \to NO_3 + M$	1.0E-32	1.0
R44	$N_2O + O(^1D) \to 2NO$	1.3	100
R45	$NO_2 + NO_3 + M \to N_2O_5 + M$	5E-31	1.0
R46	$N + NO \to N_2 + O$	1.3	100
R47	$H2 + O(^1D) \to OH + H$	1.2	100
R48	$CH_4 + O(^1D) \to CH_3 + OH$	1.2	100
R49	$CH_3 + O_2 + M \to CH_3O_2 + M$	1.5E-31	1.0
R50	$CH_2O + OH \to H_2O + HCO$	1.25	200
R51	$HCO + O_2 \to CO + HO_2$	1.3	140
R52	$Cl + HO_2 \to HCl + O_2$	1.5	200
R53	$CCl_4 + O(^1D) \to 4Cl + products$	1.2	100
R54	$OH + HO_2NO_2 \to H_2O + O_2 + NO_2$	1.5	270
R55	$CH_4 + O(^1D) \to H_2 + CH_2O$	1.2	100
R56	$OH + CH_3OOH \to H_2O + CH_3O_2$	1.5	200
R57	$OH + OH \to H_2O + O$	1.4	240
R58	$ClO + OH \to Cl + HO_2$	1.5	150
R59	$HOCl + OH \to H_2O + ClO$	3.0	500
R60	$Cl + CH_2O \to HCl + HCO$	1.15	100
R61	$HO_2 + HO_2 + M \to H_2O_2 + M$	1.3	400
R62	$CFClO + O(^1D) \to products$	2.0	100
R63	$CF_2O + O(^1D) \to products$	2.0	100
R64	$Cl + HO_2 \to OH + ClO$	2.0	200

Table 1. (continued)

Parameter	Description	f_{298} or Δk_0^{300}	$\Delta E/R$ or Δn
R65	$BrO + NO \rightarrow NO_2 + Br$	1.15	130
R66	$HO_2NO_2 + M \rightarrow HO_2 + NO_2 + M$	5.0	1000
R67	$NO + NO_3 \rightarrow 2NO_2$	1.3	100
R68	$OH + CH_3CCl_3 \rightarrow 3Cl + products$	1.1	150
R69	$NO + O + M \rightarrow NO_2 + M$	2.0E-32	0.3
R70	$N_2O + O(^1D) \rightarrow N_2 + O_2$	1.3	100
R71	$CF_2Cl_2 + O(^1D) \rightarrow ClO + Cl + fragment$	1.3	100
R72	$N + NO_2 \rightarrow N_2O + O$	1.5	100.
R73	$CFCl_3 + O(^1D) \rightarrow ClO + 2Cl + fragment$	1.2	100
R74	$O_2 + O_2(^1D) \rightarrow 2O_2$	1.2	100
R75	$O_3 + O_2(^1D) \rightarrow 2O_2 + O$	1.2	500
R76	$Br + O_3 \rightarrow BrO + O_2$	1.2	200
R77	$Br + HO_2 \rightarrow HBr + O_2$	2.0	600
R78	$BrO + ClO \rightarrow Br + ClOO$	1.25	200
R79	$BrO + BrO \rightarrow 2Br + O_2$	1.25	150
R80	$OH + HBr \rightarrow H_2O + Br$	1.2	250
R81	$BrO + NO_2 + M \rightarrow BrONO_2 + M$	6E-32	0.8
R82	$CH_3Br + OH \rightarrow Br + products$	1.1	150
R83	$CHClF_2 + OH \rightarrow Cl + 2f + products$	1.1	150
R84	$C_2Cl_3F_3 + O(^1D) \rightarrow 3Cl + products$	2.0	100
R85	$C_2Cl_2F_4 + O(^1D) \rightarrow 2Cl + 4f + products$	2.0	100
R86	$C_2ClF_5 + O(^1D) \rightarrow Cl + 5f + products$	1.3	100
R87	$ClO + ClO + M \rightarrow Cl_2O_2 + M$	4E-33	0.5
R88	$BrO + ClO \rightarrow Br + OClO$	1.25	200
R89	$BrO + ClO \rightarrow BrCl + O_2$	1.25	200
R90	$BrO + O \rightarrow Br + O_2$	1.5	150
R91	$BrO + HO_2 \rightarrow HOBr + O_2$	1.5	500
R92	$Br + CH_2O \rightarrow HBr + CHO$	1.3	200
R93	$CH_4 + O(^1D) \rightarrow H + CH_3O$	1.2	100

Read 5E-35 as 5×10^{-35}.

Table 2 lists the 45 photolytic reactions whose uncertainties are propagated through the model in this study. The uncertainty distributions for 27 of the reactions were generated from the cross-section uncertainty estimates listed by *DeMore et al.* [1994, Table 5]. For the remaining reactions, an uncertainty of $f_\sigma = 1.2$ was arbitrarily chosen. The cross-section uncertainties were applied at all wavelengths. The lognormal probability distribution characterizing the cross section uncertainty was generated similarly to the lognormal distribution characterizing k_{298} discussed above. We assumed that the uncertainty in the logarithm of the cross section was characterized by a mean value $\ln(\sigma^0(\lambda))$ where σ^0 is the nominal cross section value and λ is the wavelength, and standard deviation $\ln(f_\sigma)$. We also assumed that the solar flux was uncertain by a factor $f_{sf} = 1.1$, and varied its value accordingly in each Monte Carlo run.

Table 3 lists the heterogeneous reaction parameters whose uncertainties are propagated through the model in this study. In addition to the surface reaction probabilities we also consider the size distributions of the Type 1 and Type 2 PSCs to be uncertain and the supersaturation required before the PSCs form. The uncertainties listed in Table 3 were mostly taken from *DeMore et al.* [1994, Table 59]. However, *DeMore, et al.'s* table did not provide uncertainty estimates for several of the reaction parameters. For these cases we chose an uncertainty based on a reading of the *DeMore et al.* [1994] table notes, personal communication with laboratory experimentalists (D. Hanson, personal communication, 1996), or primary laboratory measurement sources. These cases are indicated in footnotes to Table 3.

Note that the conclusions of this paper are valid only to the extent that the characterization of the input parameter uncertainties described above is reasonable. If this is not the case, then the output uncertainty determined from the Monte Carlo runs will not reflect the actual uncertainty in the model results.

3.2. Latin Hypercube Sampling

Consider the uncertainty propagation of a single input parameter. A set of N values for the parameter are chosen and the model is run N times, once for each value. The variance in the model output of interest for the N-run set characterizes its uncertainty due to the input parameter. To be valid, the set of N input parameter values used in the runs must correctly represent the uncertainty of the input parameter. If a model run requires significant computer time, then N must be made as small as possible in order for the study to be practical. However, it must still be large enough for

Table 2. Photolytic Decomposition Rates Varied in Monte Carlo Runs

Parameter	Description	Uncertainty
J1	$O_2 \rightarrow O + O$	1.20
J2	$O_3 \rightarrow O_2 + O(^1D)$	1.25
J3	$O_3 \rightarrow O_2 + O$	1.10
J4	$H_2O \rightarrow H + OH$	1.20
J5	$NO_3 \rightarrow NO_2 + O$	2.00
J6	$HNO_3 \rightarrow OH + NO_2$	1.30
J7	$NO_2 \rightarrow NO + O$	1.20
J8	$H_2O_2 \rightarrow 2OH$	1.30
J9	$N_2O_5 \rightarrow NO_2 + NO_3$	2.00
J10	$CH_2O \rightarrow HCO + H$	1.20
J11	$CH_2O \rightarrow H_2 + CO$	1.20
J12	$CO_2 \rightarrow CO + O$	1.20
J13	$CH_3OOH \rightarrow CH_3O + OH$	1.50
J14	$N_2O \rightarrow N_2 + O$	1.20
J15	$ClONO_2 \rightarrow Cl + NO_3$	1.30
J16	$NO \rightarrow N + O$	1.20
J17	$NO_3 \rightarrow NO + O_2$	1.30
J18	$HCl \rightarrow H + Cl$	1.10
J19	$CCl_4 \rightarrow 4Cl + \text{fragment}$	1.10
J20	$CH_3Cl \rightarrow CH_3 + Cl$	1.10
J21	$CFCl_3 \rightarrow 3Cl + \text{fragment}$	1.10
J22	$CF_2Cl_2 \rightarrow 2Cl + \text{fragment}$	1.10
J23	$HOCl \rightarrow OH + Cl$	1.40
J24	$HO_2NO_2 \rightarrow OH + NO_3$	2.00
J25	$H_2O \rightarrow H_2 + O(^1D)$	1.20
J26	$CH_3CCl_3 \rightarrow 3Cl + \text{fragment}$	1.20
J27	$BrO \rightarrow Br + O$	1.20
J28	$BrONO_2 \rightarrow Br + NO_3$	1.40
J29	$CH_3Br \rightarrow CH_3 + Br$	1.20
J30	$CF_3Br \rightarrow Br + 3F + \text{fragment}$	1.30
J31	$CF_2ClBr \rightarrow Br + Cl + 2f + \text{fragment}$	2.00
J32	$CHClF_2 \rightarrow Cl + 2f + \text{fragment}$	1.20
J33	$C_2Cl_3F_3 \rightarrow 3Cl + 3f + \text{fragment}$	1.20
J34	$C_2Cl_2F_4 \rightarrow 2Cl + 4f + \text{fragment}$	1.20
J35	$C_2ClF_5 \rightarrow Cl + 5f + \text{fragment}$	1.20
J36	$Cl_2O_2 \rightarrow Cl + ClOO$	1.20
J37	$BrCl \rightarrow Br + Cl$	1.20
J38	$CO_2 \rightarrow CO + O(^1D)$	1.20
J39	$HO_2NO_2 \rightarrow HO_2 + NO_2$	2.00
J40	$CClFO \rightarrow Cl + f + \text{fragment}$	1.20
J41	$CF_2O \rightarrow 2f + \text{fragment}$	1.30
J42	$CH_4 \rightarrow CH_3 + H$	1.20
J43	$CH_4 \rightarrow CH_2 + H_2$	1.20
J44	$CH_4 \rightarrow CH + H + H_2$	1.20
J45	$CH_3O_2 \rightarrow CH_3 + O_2$	1.20

the input parameter uncertainty to be well sampled. It is therefore important to find an efficient method for selecting the input parameter values.

Consider two different techniques. The first is to randomly pick N input parameter values such that the probability of obtaining a particular value is equivalent to the probability that it is the true value of the parameter. The second method is to divide the input parameter range into N equal-probability segments and take one input parameter value from each segment. The first method is known as random sampling (RS) and the second, when generalized to multiple input parameters, is known as Latin hypercube sampling (LHS) [e.g., McKay et al., 1979]. It has been found that the number

of model runs necessary to obtain a good characterization of the uncertainty in an output parameter can be significantly smaller when LHS is used to choose the input parameter sets. This is because the LHS technique ensures that each input parameter is sampled over its entire range with the appropriate probability distribution in fewer runs than are necessary for random sampling. While LHS has not been proved to be better than RS in general, we chose this method on the basis of its demonstrated superiority in the McKay et al. [1979] study. We show below that the error in our application is slightly smaller than would be expected from a RS approach.

To use LHS with M input parameter values and N

Table 3. Heterogeneous Reaction Parameters Varied in Monte Carlo Runs

Parameter	Description	Uncertainty
H1	$ClONO_2 + HCl \rightarrow HNO_3 + Cl_2$ (sulfate)	5 [a]
H2	$ClONO_2 + H_2O \rightarrow HNO_3 + HOCl$ (sulfate)	3 [a]
H3	$N_2O_5 + H_2O \rightarrow 2HNO_3$ (sulfate)	2
H4	$HOCl + HCl \rightarrow H_2O + Cl_2$ (sulfate)	3 [b]
H5	$BrONO_2 + H_2O \rightarrow HNO_3 + HOBr$ (sulfate)	2 [c]
H6	$HOBr + HCl \rightarrow H_2O + BrCl$ (sulfate)	3 [c]
H7	$ClONO_2 + HCl \rightarrow HNO_3 + Cl_2$ (NAT)	3
H8	$ClONO_2 + H_2O \rightarrow HNO_3 + HOCl$ (NAT)	10 [a]
H9	$N_2O_5 + H_2O \rightarrow 2HNO_3$ (NAT)	3
H10	$N_2O_5 + HCl \rightarrow HNO_3 + ClONO$ (NAT)	2
H11	$HOCl + HCl \rightarrow H_2O + Cl_2$ (NAT)	3
H12	$ClONO_2 + HCl \rightarrow HNO_3 + Cl_2$ (ice)	2 [b]
H13	$ClONO_2 + H_2O \rightarrow HNO_3 + HOCl$ (ice)	10
H14	$N_2O_5 + H_2O \rightarrow 2HNO_3$ (ice)	3
H15	$HOCl + HCl \rightarrow H_2O + Cl_2$ (ice)	3
H16	$HOBr + HCl \rightarrow H_2O + BrCl$ (ice)	3
H17	Type 1 (NAT) mode radius	2 [d]
H18	Type 2 (ice) mode radius	2 [d]
H19	supersaturation ratio (NAT)	2 [e]
H20	supersaturation ratio (ice)	1.2 [e]

[a] Chosen on the basis of *DeMore et al.'s* [1994, Table 59] notes.
[b] D. R. Hanson (personal communication, 1996).
[c] Based on *Hanson and Ravishankara* [1995].
[d] Personal judgement of uncertainty.
[e] Corresponds to 1 K uncertainty in supersaturation temperature.

runs, the range of each of the M input parameters is first broken into N equal-probability segments. Then one input parameter value is chosen for each segment. The result is a set of M lists of values, (one for each parameter) each N values long. An input parameter set for a Monte Carlo run is obtained by picking one value at random from each of the lists and then striking that value from the list so it will not be used again. Picking the values at random minimizes correlations between different input parameters. The process is repeated until N input parameter sets are generated.

3.3. Run Specifics

In our LHS methodology we used a value of $N = 50$. That is, for each of the 158 parameters we considered, we divided the uncertainty range into 50 equal probability segments. We then constructed 50 input parameter sets by picking a value at random from each of the 50-value lists and then striking the value so it could not be picked again. We repeated this process nine times to obtain a total of 450 input parameter sets. This "replicated LHS" procedure [*Iman and Conover*, 1980] was adopted to allow us to evaluate the error in our predictions of model uncertainty, as explained below. Of the 450 runs we attempted, 419 were completed successfully and 31 runs failed. The largest number of failed model runs for any 50 run replication was 6. We did not attempt to rerun the failures with a modified code because we felt a failure rate of $< 10\%$ would have a minimal impact on our results and we wanted to ensure

that the model formulation was the same in all of the runs. Each run was initialized in 1970 using the same initial conditions and run for 26 years, through the end of 1995. Each run used a different input parameter set. Since the model adjusts to changes in input parameters within about 5 years, the study period after 1979 should not be affected by the model initialization. During the course of each 26-year run, source gas boundary conditions at the ground were time-stepped as described by *Jackman et al.* [1996]. Increases in chlorofluorocarbon emissions result in an increased stratospheric chlorine loading, contributing to the changes in O_3 concentrations which are the subject of this paper.

From 1970 to 1979, the sulfate aerosol distribution was set to 1979 values for the appropriate month. From 1979 to 1995 the aerosol distribution was specified from the sulfate aerosol time series mentioned above. Also as mentioned above, a parameterization of the 11-year variation in the solar ultraviolet flux was also included in each run.

It is important to determine whether or not the number of Monte Carlo calculations made for this study is adequate. Imagine a Monte Carlo study with a very large number of runs. Each run gives a prediction for the model output of interest, which for example might be the percent change in globally and annually averaged total O_3 between 1979 and 1992. As the number of runs becomes infinitely large, a limiting distribution for the model output with a mean value μ and a standard deviation σ will be formed. Each model run produces a

single sample of this limiting distribution. The σ characterizes the uncertainty in the model output and is the quantity we attempt to estimate from a finite number of Monte Carlo runs.

In the case where the model input variables are chosen at random, each Monte Carlo run will be a random sample of the model output distribution. If N Monte Carlo runs are made, a mean μ_N and standard deviation σ_N can be calculated to estimate μ and σ. The standard error of these estimates is simply $\sigma/N^{1/2}$. This suggests that with $N = 419$, the μ_N and σ_N from a random sampling Monte Carlo calculation will be within about 5% of μ and σ. If LHS provides no benefit over RS, then this is typical of the error in our uncertainty estimates.

The replicated LHS technique allows us to quantify the error in our predictions of σ because we have nine independent 50-run estimates of σ. The best estimate of σ will be the average of the nine σ_N, and the error will be given by the standard error of $\overline{\sigma_N}$. Consider for example the change in globally and annually averaged total O_3 between 1979 and 1992. The nominal value for this model output is -5.75%. The average $\overline{\sigma_N}$ =2.66%, with a standard error of 0.11%. Therefore the error in our estimate of σ is about 4.1%, which is consistent with the error we would expect from a RS Monte Carlo approach and is sufficient for the purposes of this paper.

4. Results

4.1. Total Ozone Trends

Figure 1 compares the time series of the percent change in model annually averaged global total O_3 since 1979 with observations made by the TOMS instrument.
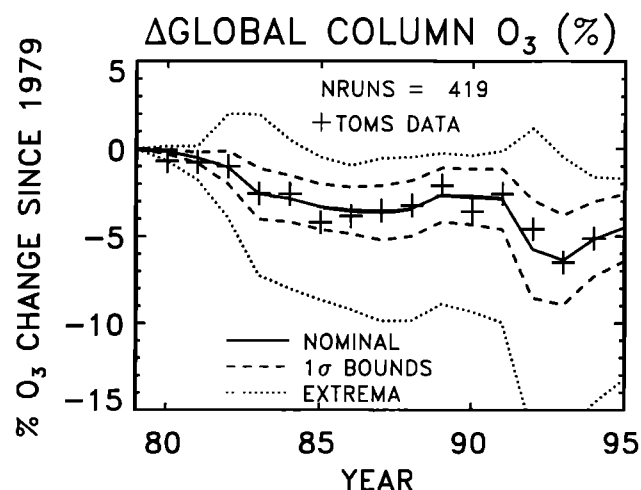

Figure 1. Percent change in the GSFC two-dimensional model annually and globally (65°S to 65°N) averaged total O_3 since 1979 compared with observations made by the TOMS instrument. The solid line is the model simulation using nominal rates, the dashed lines indicate the ±1σ variation calculated from the 419 model runs analyzed in this study, and the dotted lines indicate the high and low extreme cases. The crosses represent annually and globally averaged TOMS data.

The model result using nominal input values is the solid line, while the TOMS observations are shown by the crosses. (Note that the nominal case corresponds to the median rather than the mean of the Monte Carlo runs.) The dashed lines above and below the model nominal case indicate plus and minus 1 standard deviation from the nominal values. The dotted lines on the plot show the high and low extrema of the Monte Carlo cases. Figure 1 shows that the agreement between TOMS values and the nominal case is very good. The agreement is significantly better than would occur if solar cycle and sulfate aerosol variability were not included in the calculation, as shown by Jackman et al. [1996]. There is some disagreement between the model and observations due to year-to-year variability in the observations which does not occur in the model. Neither interannual dynamical variability nor the quasi-biennial oscillation are included in the model formulation, which could account for some of the discrepancy.

The uncertainty in the model time series resulting from uncertain input parameters is substantial. For instance, the percent change in global total O_3 between 1979 and 1993 (the year of the maximum percent change from 1979) is about 6.5% ± 2.5% (1σ), indicating that the nominal model trend and the actual model trend (the trend the model would calculate if it were supplied a correct set of input parameter values) differ in relative terms by at most 40% with a likelihood of about 2 in 3. Figure 1 also shows that the typical model/observation discrepancy is significantly smaller than the 1σ error in the model time series. The relatively large model uncertainty indicates that these differences could easily be due to errors in the input reaction rates, and it can thus be argued that the differences between the TOMS data and the nominal model time series seen in Figure 1 are insignificant. This is essentially equivalent to the statement that the good agreement between the nominal model time series and the TOMS time series could be fortuitous: it might easily be that the model/measurement discrepancy would increase if the model were given the correct set of input parameter values as input.

As mentioned above, the TOMS time series is influenced by interannual dynamical variations which do not occur in the model. This complicates the comparison of the observed and modeled changes in total O_3 resulting from the buildup of chlorine in the stratosphere. In order to compare more directly the observed and calculated trend in O_3 resulting from chlorine increases, we have fit the total O_3 time series from each of the Monte Carlo runs to a function similar to that used in the standard trend analysis of TOMS total O_3 data using the same regression technique [McPeters et al., 1996]. We can then directly compare the model trend in O_3 with the TOMS trend. Figure 2 compares the globally and annually averaged total O_3 trend from the Monte Carlo runs with the trends calculated from the TOMS data. The histogram in the figure shows the distribution of
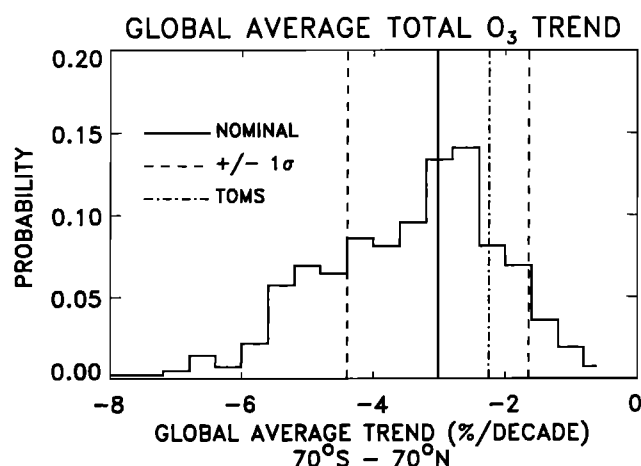
GLOBAL AVERAGE TOTAL O_3 TREND

Figure 2. Globally and annually averaged total O_3 trends from the Monte Carlo runs compared with trends derived from the TOMS data. Shown is a histogram of the Monte Carlo run results grouped into 0.4 % decade^{-1} bins. The histogram gives the probability that a Monte Carlo run resulted in a particular trend in globally and annually averaged total O_3. The solid vertical line is the trend for the nominal case, the dashed lines show the $\pm 1\sigma$ variation in the Monte Carlo runs, and the dashed-dotted line indicates the TOMS result.

the globally averaged model O_3 trend produced by the 419 Monte Carlo runs. The histogram shows the probability that a Monte Carlo run produces a trend of a certain magnitude, resolved to a bin size of 0.4 percent per decade. The solid vertical line in the figure marks the nominal case trend of -3.02 % decade^{-1}, and the dashed vertical lines show the $\pm 1\sigma$ variation of 1.38 % decade^{-1} around the nominal result. The dashed-dot vertical line shows the TOMS result of -2.26 % decade^{-1}. The plot shows that the nominal model case is about 34% larger than the TOMS trend and that the two lie within the 1σ uncertainty in the model result. This demonstrates more convincingly than the time series comparison above that the difference between the model and the TOMS trend is not significant. Errors in the nominal input parameter set could relatively easily be hiding better (or worse) model/measurement discrepancies.

Figure 3 shows the time series of annually averaged total O_3 at 45° N and 45° S, again in terms of the percent change since 1979. The same plotting symbols are used here as in Figure 1. We have also included a 2-year running average of the TOMS data on the plot to smooth out the interannual and biannual variability and focus on the decadal time scales. This comparison tests the model more stringently than the globally averaged total O_3 comparison shown in Figure 1 because of the larger influence of transport processes on column O_3 at higher latitudes. Again we see very good agreement between the model nominal case and the TOMS observations. The discrepancies due to 1- and 2- year interannual variations are larger in these plots than in the globally averaged case, but overall the model/measurement

agreement is good enough to be considered fortuitous given the uncertainty in the model time series from the Monte Carlo runs.

To focus on the annually averaged O_3 trend as a function of latitude we compare in Figure 4 the TOMS and model annually averaged total O_3 trends as a function of latitude obtained using the regression model described above. As before, the solid line represents the nominal case, the dashed lines show the $\pm 1\sigma$ variation from the nominal case, and the crosses represent the TOMS data. Considering the model uncertainty in the tropics, there is a statistically significant difference (at the 1σ level) between the nominal trend of about 2 % decade^{-1} and the TOMS values. However, the TOMS-calculated trends are also uncertain, and it is possible that errors in both the model calculations and the TOMS data produce the discrepancy between the model nominal result and the TOMS trend.

Figure 4 shows that the model nominal annually averaged O_3 trend and the TOMS-derived trend agree very well in the northern hemisphere midlatitudes. However, the figure also shows that the uncertainty in
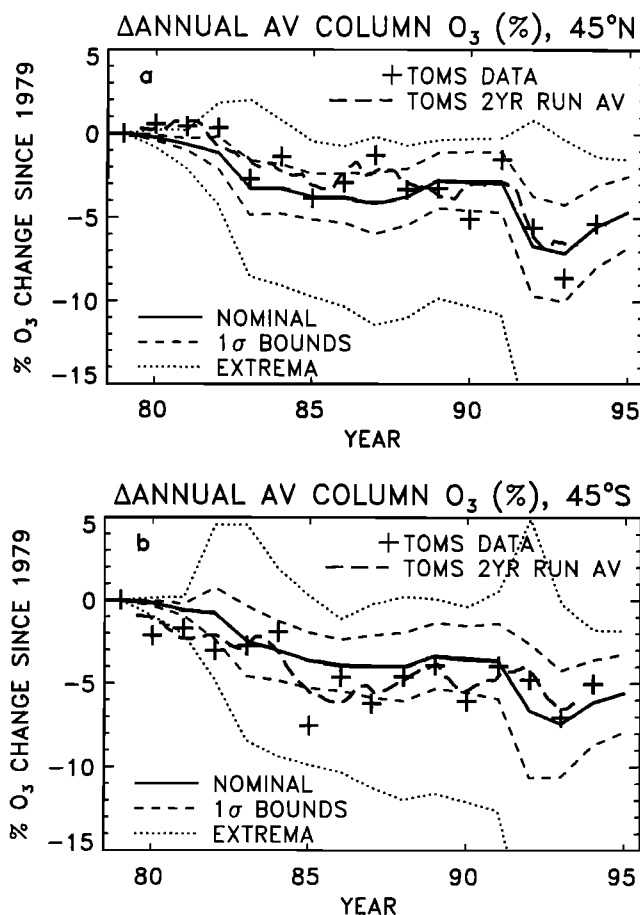
ΔANNUAL AV COLUMN O_3 (%), 45°N

ΔANNUAL AV COLUMN O_3 (%), 45°S

Figure 3. Percent change since 1979 of annually averaged total O_3 for the GSFC 2-D model at 45° N and 45° S compared to TOMS observations. The solid, dashed, and dotted lines, as well as the crosses, are as in Figure 2. The long dashed line shows a 2-year running average of the TOMS data.
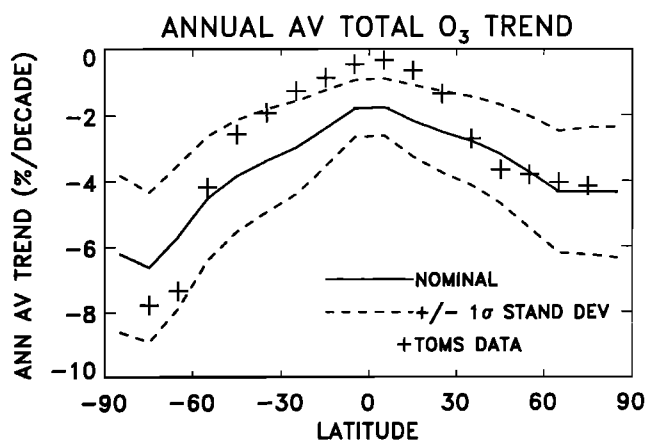
Figure 4. Latitude dependence of the annually averaged trend in total O_3, (% decade^{-1}). The solid line shows the modal nominal case, the dashed lines indicate the $\pm 1\sigma$ uncertainty in the result calculated from the Monte Carlo runs, and the crosses indicate the annually averaged trend in total O_3 calculated from the TOMS data.

the model result at these latitudes is large. For instance, at 55°N the model annually averaged O_3 trend is 3.8 ± 1.8 % decade^{-1}, an uncertainty of about 47%. Because of this large uncertainty, the good agreement between the model and the observations is meaningless. It could easily be that errors in one the nominal input parameters are fortuitously countering a model formulation error which would be apparent if the correct input parameter values were used.

An obvious difference between the model and TOMS annually averaged total O_3 trends shown in Figure 4 is the meridional gradient of the trend, which is significantly larger in the TOMS observations than in the model nominal case. The difference between the model and the observations can be examined more closely by calculating the meridional gradients in each of the Monte Carlo runs and comparing the variability in the gradient with the difference between the model and TOMS gradients. Figure 5 shows this comparison. The model meridional gradient of the annually averaged total O_3 trend (percent per decade per degree latitude) is plotted with its $\pm 1\sigma$ variability and is compared to the gradients in the TOMS annually averaged trends. The largest disagreements between the model nominal case and the TOMS results occur in the northern hemisphere at 35° and in the southern hemisphere at -55°. Both the northern and southern hemisphere model/measurement discrepancies are about 4 to 5 times the 1σ uncertainty in the model gradient. These discrepancies are so large that it is unlikely that errors in the nominal input parameter set could be responsible for the large model/observation discrepancy. The weak model meridional gradients seen in the model are therefore likely to be due instead to errors in the model transport formulation.

Two-dimensional models have well-known problems in correctly capturing the characteristics of meridional transport in the atmosphere. These models often overestimate the amount of mixing between the tropics and midlatitudes, and between the midlatitudes and the polar vortex during winter [Bacmeister et al., 1995; Fahey et al., 1996]. It is thus not surprising that such a model would poorly represent the meridional gradients in the O_3 trends. The model/measurement discrepancy seen in Figure 5 illustrates how a well-known model transport problem is revealed in this uncertainty analysis. Similar sorts of discrepancies may point to other less understood model formulation problems.

4.2. Seasonal Total Ozone Trends

Total O_3 trends vary significantly over the course of the year and it is important to understand the factors contributing to this variation. Figure 6a shows the seasonal and meridional variation of Earth's total O_3 as calculated from version 7 TOMS data from instruments on the Nimbus 7 and Meteor 3 satellites between November 1978 and October 1994. Conclusions concerning a model's ability to capture the trends in total O_3 are typically drawn from such a plot. Figure 6b shows the corresponding result from the the GSFC 2-D model for the nominal input parameter set. Note that this differs slightly from that presented by Jackman et al. [1996] due to a somewhat different transport formulation in the two simulations.

Figure 6c shows the 1σ uncertainty of the model calculation. This figure can be used to determine the significance of the discrepancies between the TOMS and model total O_3 trends shown in Figures 6a and 6b,
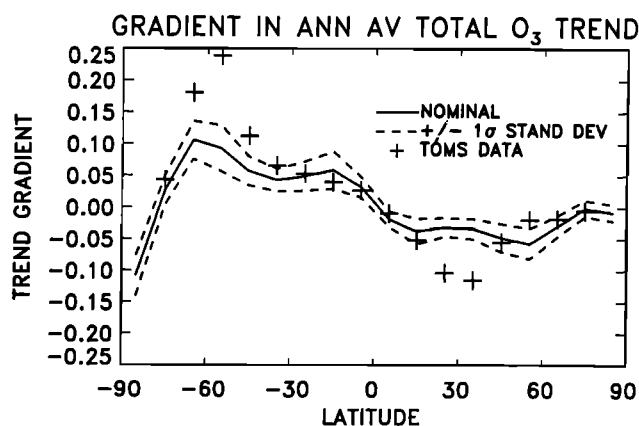

Figure 5. Meridional gradient in annually averaged trend in total O_3 calculated by the GSFC 2-D model, its uncertainty from the Monte Carlo runs, and comparison to TOMS observations. The solid line shows the nominal case gradient in the annually averaged total O_3 trend, in % decade^{-1} (degree latitude)$^{-1}$. The dashed lines show the $\pm 1\sigma$ variation in the gradient calculated using the Monte Carlo runs. The crosses show the trend gradients calculated using Nimbus 7 and Meteor 3 TOMS observations.
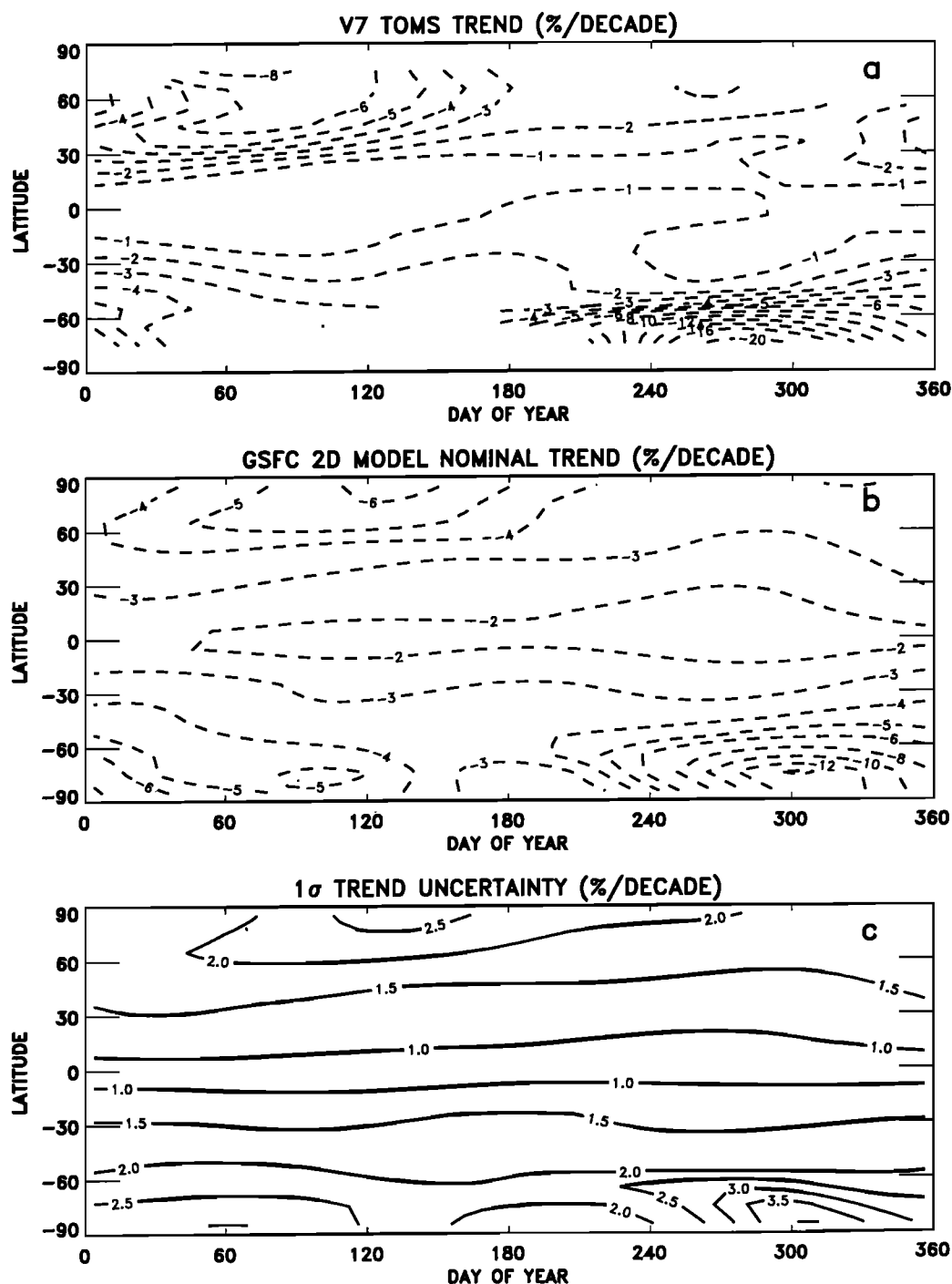
Figure 6. Meridional and seasonal dependence of the TOMS total O_3 trends, and model-calculated total O_3 trends and trend uncertainty. (a) TOMS trends calculated from version 7 Nimbus 7 and Meteor 3 TOMS data in % decade^{-1}. (b) The model trend using nominal values of the input parameters and the same statistical model as in the TOMS calculations, minus a QBO term. (c) Monte Carlo estimate of the uncertainty in the model-calculated total O_3 trend (% decade^{-1}).

respectively. Figure 6c shows that the smallest uncertainties occur in the tropics, while the largest occur in the late spring/early summer in both the northern and southern hemispheres. The maximum uncertainty occurs in the southern hemisphere high latitudes where the model calculates the largest trends in total

O_3. Note, however, that as a fraction of the model-calculated trend, the southern hemisphere high-latitude uncertainty is actually a minimum, with the trend uncertainty as low as 25% of the trend itself. The maximum relative uncertainty of about 70% occurs at southern high latitudes in midwinter. Throughout most of
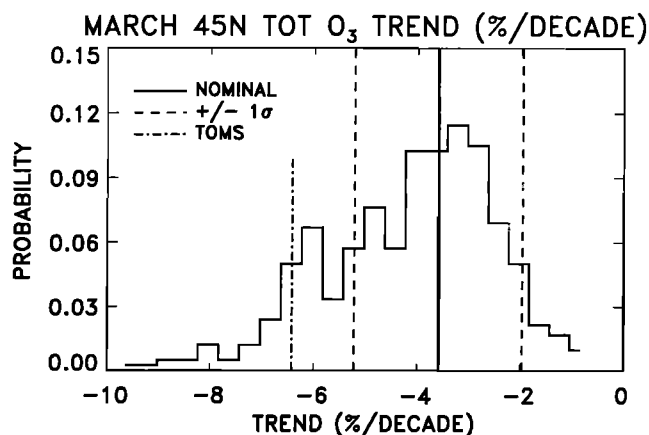
MARCH 45N TOT O_3 TREND (%/DECADE)

Figure 7. Probability distribution of total O_3 trend calculations for March at 45°N from the Monte Carlo runs compared to the observed trend. Shown is a histogram of 419 model calculations divided into 0.4 % decade^{-1} bins and normalized to be expressed as a probability. The model result using nominal input parameter values is the solid vertical line. The dashed lines show the $\pm1\sigma$ values. The dot-dash line shows the total O_3 trend calculated with TOMS data for March at 45°N.

the year and over most of the globe, however, the relative uncertainty in the model is trend is fairly uniform, varying between 35% and 50%.

It is often noted that models significantly underestimate total O_3 trends in the northern hemisphere midlatitudes in March [e.g., *Solomon et al.*, 1996]. The Monte Carlo calculation allows us to determine whether there really is a significant difference between the model calculation and the observations, or whether the discrepancy might easily be due to an error in the nominal model input parameters. Figure 7 is a plot of the probability distribution of the Monte Carlo runs for the middle of March, at 45°N. As before, the Monte Carlo runs are distributed into bins with a width of 0.4 % decade^{-1}. The solid vertical line indicates the model nominal trend of -3.59 % decade^{-1}. The dashed vertical lines indicate the $\pm1\sigma$ variation around the nominal case of 1.63 % decade^{-1}. The dash-dot vertical line indicates the TOMS trend value of -6.42 % decade^{-1}. The plot shows that the difference between the model nominal case and the TOMS trend is significant at the 1σ level but not at 2σ. It is thus possible, but not very likely, that the discrepancy between the model nominal case and the TOMS data results from an error in the nominal case input parameters. One might refer to the model/measurement discrepancy in this case as being marginally significant. It is important to remember, however, that the uncertainty calculated from these Monte Carlo calculations does not include variations in the model transport formulation as a source of model uncertainty and is a lower bound to the total uncertainty in the model calculation. It is possible that the combination of dynamical and input uncertainties

would be large enough to render the differences between the model and the observed total O_3 trends insignificant at this latitude and time of year.

One fairly obvious difference between the TOMS trends shown in Figure 6a and the model trends in 6b is a much larger seasonal variation in the observed trend than the model calculated trend. We note that a weak seasonal trend variability is a common model problem [*World Meteorological Organization*, 1995]. To examine this more closely we plot in Figure 8 the seasonal amplitude of the total O_3 trend as a function of latitude, where the amplitude is calculated as the difference between the maximum trend and the minimum trend at a particular latitude. The trend amplitude for the model nominal case is the solid line, the dashed lines show the $\pm1\sigma$ variation around the nominal case, and the crosses show the TOMS trend amplitudes. Figure 8 shows that the model underestimates the trend amplitude at most latitudes, but is particularly far from the mark in the northern hemisphere midlatitudes. Figure 8 also shows that the trend amplitude does not vary much between the Monte Carlo runs, so the difference between the model nominal case and the TOMS seasonal trend amplitude is up to 8.75 times σ at 45°. In contrast to the discrepancy between the measured and modeled global total O_3 trend (Figure 2) or the March midlatitude total O_3 trend (Figure 7), this is a clear case where it is extremely unlikely that the difference between the model and the TOMS result is caused by an input parameter error. Here it is very clear that the model formulation is incorrect, and resources can confidently be directed toward a real as opposed to a possible model problem.

4.3. Sources of Uncertainty

The Monte Carlo methodology provides a good estimate of the uncertainty of model output given a good

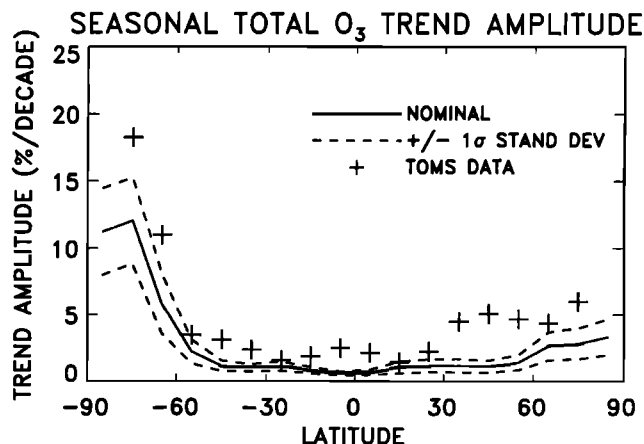## SEASONAL TOTAL O_3 TREND AMPLITUDE

Figure 8. Seasonal total O_3 trend amplitude as a function of latitude. The amplitude is defined as the difference between the maximum and the minimum trend in total O_3 at a particular latitude. The nominal case, $\pm1\sigma$ variation, and TOMS values are indicated by the solid line, dashed lines, and crosses, respectively.

characterization of the uncertainty in the model input parameters. However, the technique does not directly calculate which of the input parameters contribute strongly to the model output uncertainty and which do not. In this section we attempt to determine indirectly which parameters have the largest influence on the model output uncertainty.

Two factors determine the importance of the uncertainty in an input parameter to the model output uncertainty: (1) the sensitivity of the model output to changes in that parameter, and (2) the magnitude of the input parameter uncertainty. If the model output of interest is insensitive to the input parameter, it does not matter how uncertain the value of that parameter is. On the other hand, a very precisely and accurately measured input parameter may not contribute greatly to the model output uncertainty even if there is a large sensitivity.

A typical strategy for determining the contribution of the model input parameters to the model output uncertainty in a Monte Carlo study is to fit the model output to an analytic function of the input parameters using a regression technique [e.g., *Gao et al.*, 1996; *Stewart and Thompson*, 1996]. The standard fitting function assumes a linear relationship between each input parameter and the output of interest. Thus

$$y = a_0 + a_1 p_1 + a_2 p_2 + \ldots + a_m p_m, \qquad (8)$$

where y is the model output of interest, $p_1, \ldots, p_m$ are the fitting parameters, and $a_0, \ldots, a_m$ are the coefficients obtained from the regression analysis characterizing the linear relationship between the input parameter and the model output. There is no guarantee that this method will work everywhere in the model domain and at all times. However, as shown below, the fit is often reasonable.

If the fit is good, then standard error propagation suggests that the contribution of the variance of each input parameter to the variance in the output can be approximated by

$$\sigma_y^2 \approx \left(\frac{\partial y}{\partial k_1}\right)^2 \sigma_1^2 + \left(\frac{\partial y}{\partial k_2}\right)^2 \sigma_2^2 + \ldots. \qquad (9)$$

Given equation (8), $\partial y / \partial k_i = a_i$. To obtain a normalized result we calculate the fractional contribution of the ith parameter to the variance using

$$f_i = \frac{a_i^2 \sigma_i^2}{\sum_i a_i^2 \sigma_i^2} \qquad (10)$$

We first examine the sources of uncertainty in the northern hemisphere midlatitude spring column O_3 trends. To do this, we have fit the percent change in column O_3 between 1980 and 1990 at 45°N in March using a linear function of the input parameters as in equation (8). The change in column O_3 is most highly correlated with the reactions evaluated at the 38.5-mbar level. This is the pressure level with the largest O_3
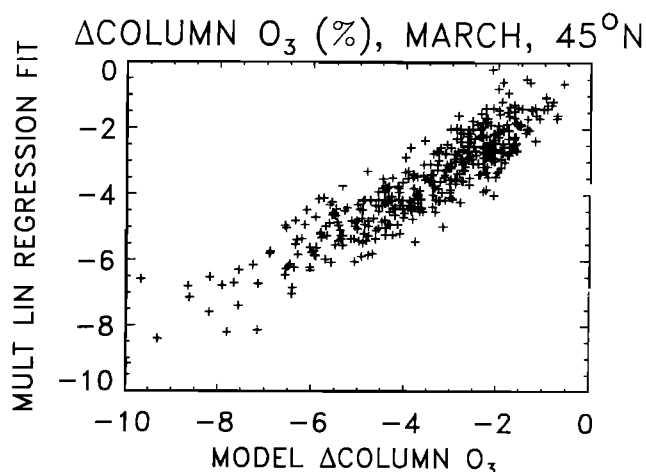

Figure 9. Comparison of model calculated 1980-1990 percent change in column O_3 at 45°N in March with predicted changes from a multiple linear regression fit to the model values. The crosses show the values for each of the 419 Monte Carlo runs.

concentration changes and hence the largest contributor to the change in column O_3. The multiple linear correlation coefficient for the fit is 0.91, indicating that the fitting equation can explain 91% of the variance in the change in column O_3 calculated in the Monte Carlo runs. The quality of the fit is shown in Figure 9, which compares the model calculated percent change in column O_3 on the x axis with the prediction of the linear relation expressed by (8) on the y axis. The points are reasonably compactly arranged along the 1-to-1 line as is required of a good fit. There is a tendency for the linear fit to underestimate somewhat the cases with the largest reductions in total O_3.

The regression results in two measures of a parameter's importance: First is the linear correlation coefficient specifying the degree to which each individual parameter correlates with the change in total O_3. Second is the fractional contribution to the total variance of the change in total O_3 calculated from the multiple linear regression fit, as in equation (10). The parameters which are most highly correlated with the change in total O_3 also tend to be the largest contributors to the variance. Only a few of the fitted parameters have either high correlation coefficients or large fractional contributions to the total variance. There is also a significant correlation between the two: if a parameter has a large correlation coefficient, it tends also to be a strong contributor to the variance. This implies that only a few of the parameters control the response of model total O_3 distributions to changes in chlorine loading.

Table 4 shows the 11 parameters which have an absolute linear correlation coefficient larger than 0.1 and a fractional contribution to the variance larger than 2%. For a 419-run data set, the probability that a correlation coefficient exceeds 0.1, 0.15, and 0.2 simply by chance is about 4%, 0.2%, and 0.004%, respectively. Thus it is

Table 4. Regression Analysis of March 1980-1990 Percent Change in Column O_3 at 45° N

Number	Parameter	Correlation	Contribution to Variance (%)
1	$N_2O + O(^1D) \rightarrow NO + NO$	0.350	15.19
2	$HNO_3 + OH \rightarrow NO_3 + H_2O$	0.295	12.06
3	$HCl + OH \rightarrow Cl + H_2O$	-0.289	6.84
4	$O_3 + OH \rightarrow HO_2 + O_2$	0.273	3.50
5	$N_2O_5 + h\nu \rightarrow NO_2 + NO_3$	0.272	12.02
6	$N_2O_5 + H_2O \rightarrow 2HNO_3$ (sulfate)	-0.259	3.76
7	$N_2O_5 + M \rightarrow NO_2 + NO_3 + M$	0.198	2.03
8	$NO_2 + O_3 \rightarrow NO_3 + O_2$	-0.194	4.50
9	$Cl + O_3 \rightarrow ClO + O_2$	-0.187	3.15
10	$N_2O + h\nu \rightarrow N_2 + O$	-0.161	2.05
11	$O_3 + h\nu \rightarrow O_2 + O(^1D)$	0.108	2.79

Analysis is based on 419 Monte Carlo runs fit to 158 input parameters at 38.5 mbar level.

likely that a physical relationship exists between these parameters and the model column O_3 change. The second column of Table 4 lists the correlation coefficents for the reactions, and the third column lists the fractional contribution of each of the tabulated parameters to the total variance in column O_3 in the linear regression fit.

Table 4 shows that ~68% of the variance in the column O_3 change from multiple linear regression fit is produced by these 11 reactions. The table also illustrates the importance of the odd nitrogen family in controlling the response of model total O_3 to chlorine perturbations. Parameter 1 is the primary producer of NO_y in the atmosphere; the more NO_y, the more increases in Cl_y will be stored in the reservoir forms via reactions of ClO with the NO_y radicals NO and NO_2. Parameter 10 would tend to reduce the amount of background NO_y and hence reduce the fraction of Cl_y in reservoir forms. Parameters 2, 5, and 7 convert reservior forms of NO_y to reactive forms which can tie up Cl_y in its reservoir forms. Parameter 8 is an essential step in the formation of HNO_3, removing forms of NO_y which can react with Cl_y species.

Parameters 3 and 9 are reactions which directly control the partitioning of Cl_y. They both force the partitioning of Cl_y toward more active forms, resulting in negative correlation coefficients. Parameter 4 also has an understandable effect, reducing the amount of OH

available to convert HCl to reactive chlorine and resulting in a positive correlation. Parameter 11 produces numerous changes which would be expected to reduce the O_3 trend such as increasing the production of HO_x and NO_y and changing the partitioning of Cl_y in favor of reservior forms. It is not obvious which of these might dominate the others.

The parameters shown in Table 4 are those which are most strongly correlated with the changes in column O_3 produced by increases in stratospheric Cl_y concentrations. It is interesting but not surprising to note that a different set of parameters are highly correlated with background O_3 concentrations. A set of nine of these parameters for 45°N, in March at 38.5 mbar, are shown in Table 5. The listed parameters have linear correlation coefficients greater than 0.1 and contribute more than 1% to the variance in the multiple linear regression fit. The multiple linear correlation coefficient for this fit is 0.96, which is better than for the fit to changes in column O_3 amounts discussed above. By far the most highly correlated parameter is O_2 photolysis, which is the primary O_x production mechanism. This parameter is itself responsible for almost 60% of the variance in background O_3 concentrations, and together these nine input parameters account for ~85% of the total variance in the O_3 levels calculated from the multiple linear regression fit.

Table 5. Regression Analysis of March O_3 at 45° N and 38.5 mbar

Number	Parameter	Correlation	Contribution to Variance (%)
1	$O_2 + h\nu \rightarrow O + O$	0.723	59.86
2	$O + O_2 + M \rightarrow O_3 + M$	0.307	10.32
3	$NO + O_3 \rightarrow NO_2 + O_2$	-0.156	1.39
4	$O_3 + h\nu \rightarrow O_2 + O$	-0.141	3.82
5	$OH + O_3 \rightarrow HO_2 + O_2$	-0.120	1.46
6	$NO_2 + O \rightarrow NO + O_2$	-0.119	2.18
7	$HO_2 + O_3 \rightarrow OH + 2O_2$	-0.115	3.67
8	$O_3 + h\nu \rightarrow O_2 + O(^1D)$	-0.106	1.26
9	$HCl + OH \rightarrow Cl + H_2O$	-0.105	1.16

Table 6. Regression Analysis of Δ Column O_3 Between 1980 and 1990 in October at 75° S

Number	Parameter	Correlation	Contribution to Variance (%)
1	$O_2 + h\nu \rightarrow O + O$	0.314	10.47
2	Type 2 aerosol radius	0.253	6.07
3	$BrO + ClO \rightarrow Br + ClOO$	-0.177	3.61
4	$N_2O + O(^1D) \rightarrow NO + NO$	0.173	4.07
5	$HNO_3 + OH \rightarrow NO_3 + H_2O$	0.171	6.87
6	$N_2O_5 + H_2O \rightarrow 2HNO_3$ (sulfate)	-0.156	2.21
7	$BrO + ClO \rightarrow Br + OClO$	-0.146	5.78
8	$HCl + OH \rightarrow Cl + H_2O$	-0.141	4.57
9	$O + O_2 + M \rightarrow O_3 + M$	0.126	3.41
10	$ClONO_2 + H_2O \rightarrow HNO_3 + HOCl$	-0.111	4.00
11	$CH_4 + Cl \rightarrow CH_3 + HCl$	0.100	2.98

Input parameters are for October at 75°S and the 39 mbar level.

The fact that different input parameters control the background O_3 concentrations and its response to Cl_y perturbations suggests that it is not possible to conclude from a model's good reproduction of observed O_3 levels that its response to a perturbation will be reliable. This should be established instead from a model's ability to reproduce observed changes in O_3.

Figure 6a shows that the largest model trends in column O_3 occur in the southern hemisphere high latitude spring. The input parameters which apparently control the sensitivity of the model southern hemisphere high-latitude region in spring are shown in Table 6. The multiple linear correlation coefficient here is about 0.81, so the regression model is less able to account for the variance in the model-calculated change in column O_3 at this location than at midlatitudes. Also, the fraction of the total variance contributed by the 11 listed parameters is $\sim$54%, lower than for the midlatitude column O_3 change discussed above.

Several of the important midlatitude northern hemisphere input parameters shown in Table 4 reappear in this table. However, the increased role of heterogeneous reactions and halogen chemistry is reflected in the appearance in the table of the Type 2 PSC radius, the $ClO + BrO$ reactions, and the heterogeneous reaction $ClONO_2 + H_2O \rightarrow HOCl + HNO_3$ on ice. The rate of this reaction has a factor of 10 uncertainty associated with it according to DeMore et al. [1994], which might explain its appearance on this list over other ice-catalyzed reactions which have larger sticking coefficients.

5. Summary and Conclusions

We have presented a Monte Carlo estimate of the uncertainty in total O_3 trend predictions made using the GSFC 2-D model. This uncertainty results from uncertainties in input gas phase and heterogeneous reaction rates, and photolysis coefficients. We have used Latin hypercube sampling to reduce the number of runs necessary to obtain a good estimate of the uncertainty.

Given this technique, the 419 runs completed for this study should result in an error of no more than a few percent.

The uncertainty in the model prediction of the globally and annually averaged trend in total O_3 is large enough such that the difference between the model prediction and the trend calculated from Nimbus 7 and Meteor 3 TOMS data is insignificant. We find a marginally significant difference between the modeled and observed equatorial annually averaged total O_3 trend which is insignificant when errors in the TOMS calculation are considered in addition to the model uncertainty. At mid to higher latitudes the difference between the measured and observed annually averaged trend in column O_3 is again insignificant. The difference between the modeled and observed total O_3 trend in March at 45°N is marginally significant when considering the uncertainty in the model calculation only. Assuming the input parameter uncertainty estimates to be true, it is possible that the differences between the model results and the observations in these cases arise from errors in the input parameters and not from an incorrect model formulation. Thus it seems that efforts to increase the agreement between the model and the observations in these cases by changing the model formulation might be wasted without more precise and accurate specification of the model input parameters.

Good agreement between a model and the observations listed above might simply be due to fortuitously compensating errors in some input parameter and the model formulation, so grading the performance of a model using such observations should also be avoided until the differences between the model results and observations can be shown to be significant.

Clearly significant differences between the modeled and observed trends are seen in the meridional gradients of the annually averaged trends at midlatitudes and the seasonal trend amplitude at all latitudes. It is quite unlikely that these differences could be caused by errors in the input parameters so it is very likely that

they are the result of an incorrect model formulation. Further model development efforts can be directed toward resolving these discrepancies.

The contribution of a particular input parameter uncertainty to the total model output uncertainty depends on both the magnitude of the input parameter uncertainty and the sensitivity of the model to that parameter. Direct information concerning the contribution of each input parameter is not available in a Monte Carlo analysis, but an approximation can be made by fitting the model output to a linear function of the input parameters and then determining the contribution of the variance in each input parameter to the total variance of the regression model fit. This technique reveals that only a few of the input parameters contribute much to the variance at any particular location. Reducing the uncertainty of those parameters would produce the largest decreases in model uncertainty. The regression analysis also shows that the parameters controlling the variance in background O_3 concentrations are not the same as the ones producing variance in the model response to Cl_y increases.

We stress that the validity of these output uncertainty calculations depends on a correct evaluation of the input parameter uncertainties. If these are generally overestimated, then the uncertainty in the model calculations will also be overestimated. There is some observational evidence to suggest that interpreting the *DeMore et al.* [1994] values as 1σ uncertainties overestimates the actual uncertainties in the tabulated rates. *Cohen et al.* [1994] made this assumption when comparing observed HO_x partitioning from aircraft observations to the predictions of a simple analytical model, and found better model/measurement agreement than was expected from the calculated uncertainties. In such a situation model/measurement discrepancies that indicate model problems might incorrectly be judged to be the insignificant consequence of input parameter errors. A more specific recommendation on how to interpret the *DeMore et al.* [1994] uncertainty estimates would be helpful in future uncertainty studies.

References

Anderson, D. E., Jr., and S. A. Lloyd, Polar twilight UV-visible radiation field: Perturbations due to multiple scattering, ozone depletion, stratospheric clouds, and surface albedo, *J. Geophys. Res.*, *95*, 7429-7434, 1990.

Bacmeister, J. T., M. R. Schoeberl, M. E. Summers, J. R. Rosenfield, and X. Zhu, Descent of long-lived trace gases in the winter polar vortex, *J. Geophys. Res.*, *100*, 11,669-11,684, 1995.

Chen, L., H. Rabitz, D. B. Considine, C. H. Jackman, and J. A. Shorter, Chemical reaction rate sensitivity and uncertainty in a two-dimensional middle atmospheric ozone model, *J. Geophys. Res.*, *102*, 16,201-16,214, 1997.

Cohen, R. C., et al., Are models of catalytic removal of O_3 by HO_x accurate? Constraints from in situ measurements of the OH to HO_2 ratio, *Geophys. Res. Lett.*, *21*, 2539-2542, 1994.

Considine, D. B., A. R. Douglass, and C. H. Jackman, Effects of a polar stratospheric cloud parameterization on ozone depletion due to stratospheric aircraft in a two-dimensional model, *J. Geophys. Res.*, *99*, 18,879-18,894, 1994.

DeMore, W. B., D. M. Golden, R. F. Hampson, C. J. Howard, C. E. Kolb, M. J. Kurylo, M. J. Molina, A. R. Ravishankara, and S. P. Sander, Chemical kinetics and photochemical data for use in stratospheric modeling, Evaluation number 11, *JPL Publ.*, *94-26*, 273 pp., 1994.

Douglass, A. R., and R. S. Stolarski, The use of atmospheric measurements to constrain model predictions of ozone change from chlorine perturbations, *J. Geophys. Res.*, *92*, 6662-6674, 1987.

Fahey, D. W., et al., In situ observations of NO_y, O_3, and the NO_y/O_3 ratio in the lower stratosphere, *Geophys. Res. Lett.*, *23*, 1653-1656, 1996.

Fish, D. J., and M. R. Burton, The effect of uncertainties in kinetic and photochemical data on model predictions of stratospheric ozone depletion, *J. Geophys. Res.*, *102*, 25,537-25,542, 1997.

Fleming, E. L., S. Chandra, C. H. Jackman, D. B. Considine, and A. R. Douglass, The middle atmospheric response to short and long term solar UV variations: Analysis of observations and 2-D model results, *J. Atmos. Terr. Phys.*, *57*, 333-365, 1995.

Gao, D., W. R. Stockwell, and J. B. Milford, Global uncertainty analysis of a regional-scale gas-phase chemical mechanism, *J. Geophys. Res.*, *101*, 9107-9119, 1996.

Hanson, D. R., and A. R. Ravishankara, Heterogeneous chemistry of bromine species in sulfuric-acid under stratospheric conditions, *Geophys. Res. Lett.*, *22*, 385-388, 1995.

Iman, R. L., and W. J. Conover, Small sample sensitivity analysis techniques for computer models, with an application to risk assessment, *Comm. Stat. A*, *9*, 1749-1874, 1980.

Jackman, C. H., E. L. Fleming, S. Chandra, D. B. Considine, and J. E. Rosenfield, Past, present, and future modeled ozone trends with comparisons to observed trends, *J. Geophys. Res.*, *101*, 28753-28767, 1996.

McKay, M. D., R. J. Beckmand, and W. J. Conover, A comparison of three methods for selecting values of input variables in the analysis of output from a computer code, *Technometrics*, *21*, 239-245, 1979.

McPeters, R. D., S. M. Hollandsworth, L. E. Flynn, J. R. Herman, and C. J. Seftor, Long-term ozone trends derived from the 16-year combined Nimbus 7 Meteor 3 TOMS Version 7 record, *Geophys. Res. Lett.*, *23*, 3699-3702, 1996.

Prather, M. J., Numerical advection by conservation of second-order moments, *J. Geophys. Res.*, *91*, 6671-6681, 1986.

Solomon, S., R. W. Portmann, R. R. Garcia, L. W. Thomason, L. R. Poole, and M. P. McCormick, The role of aerosol variations in anthropogenic ozone depletion at northern midlatitudes, *J. Geophys. Res.*, *101*, 6713-6727, 1996.

Solomon, S., R. W. Portmann, R. R. Garcia, W. Randel, F. Wu, R. Nagatani, J. Gleason, L. Thomason, L. R. Poole, and M. P. McCormick, Ozone depletion at mid-latitudes: Coupling of volcanic aerosols and temperature variability to anthropogenic chlorine, *Geophys. Res. Lett.*, *25*, 1871-1874, 1998.

Stewart, R. W., and A. M. Thompson, Kinetic data imprecisions in photochemical rate calculations: Means, medians and temperature dependence, *J. Geophys. Res., 101,* 20,953-20,964, 1996.

Stolarski, R. S., and A. R. Douglass, Sensitivity of an atmospheric photochemistry model to chlorine perturbations including consideration of uncertainty propagation, *J. Geophys. Res., 91,* 7853-7864, 1986.

Stolarski, R. S., D. M. Butler, and R. D. Rundel, Uncertainty propagation in a stratospheric model, 2, Monte Carlo analysis of imprecisions due to reaction rates, *J. Geophys. Res., 83,* 3074-3078, 1978.

Thompson, A. M., and R. W. Stewart, Effect of chemical kinetics uncertainties on calculated constituents in a tropospheric photochemical model, *J. Geophys. Res., 96,* 13,089-13,108, 1991.

World Meteorological Organization, Scientific assessment of stratospheric ozone: 1994, *Rep. 37,* Global Ozone Res. and Monit. Proj., World Meteorol. Orgon., Geneva, 1995.

D. B. Considine, 3439 Computer and Space Sciences Building, Department of Meteorology, University of Maryland, College Park, MD 20742. (e-mail: dbc@welkin.gsfc.nasa.gov)

E. L. Fleming, S. M. Hollandsworth, C. H. Jackman, and R. S. Stolarski, Code 916, NASA Goddard Space Flight Center, Greenbelt, MD 20771.